Acta Cryst. (1993). A**49**, 736–743

Interpretation of Displacement-Caused Diffuse Scattering Using the Taylor Expansion

BY B. D. BUTLER AND T. R. WELBERRY

Research School of Chemistry, Australian National University, GPO Box 4, *Canberra City, ACT* 2601, *Australia*

(*Received* 28 *September* 1992; *accepted* 1 *February* 1993)

Abstract

The suitability is considered of employing a Taylor expansion of the kinematic scattering equation for analysing and interpreting diffuse diffraction intensities induced by atomic displacements. The diffuse scattering caused by static atomic displacements in yttria-stabilized cubic zirconium oxide is used as a test of the method because a computer model of the local atomic structure exists that satisfactorily reproduces the measured diffraction data. By concentration on the computer model, it was possible to calculate the diffuse intensity using expansions to various orders and test the results against an exact computation of the diffuse diffraction pattern. In this example, where the r.m.s. atomic displacements are approximately 3%, it was found that the usual second-order expansion could not account for many diffraction features. Most notable was the inability of an expansion to second order to describe an observed asymmetry across certain reciprocal planes. Expansion to a minimum of three orders is necessary to describe such features qualitatively and an accurate quantitative fit of the diffraction pattern at moderate diffraction angles requires the use of a fourth-order expansion.

1. Introduction

Diffraction patterns from real crystals contain both the normal peaked Bragg scattering that arises from the long-range lattice periodicity and a broad (usually weak) diffuse intensity that reflects short-range deviations of the structure from the long-range average. Although, normally, emphasis is placed on the Bragg intensities, the diffuse component has long been the subject of study because local atomic arrangements that deviate from the average often give rise to important physical properties. Unfortunately, the diffuse diffraction pattern can be difficult to interpret because, inevitably, information regarding both the local chemical pair correlations and the *distribution* of static and thermal atomic displacements will contribute to the total scattering.

In early studies of short-range order in alloys (Cowley, 1950), the effect of static atomic displacement was neglected and the total diffuse intensity was treated as arising only from short-range chemical order. This interpretation was known to be in error because of a clear asymmetry across Bragg peaks observed in the diffraction patterns of the alloys being studied. This asymmetry results from static atomic distortions associated with local ordering. These distortions, often called atomic size-effect displacements, were partially accounted for by Warren, Averbach & Roberts (1951), who employed an analysis method based on a Taylor expansion to first order in atomic displacement of the complex exponential in the kinematic scattering equation. The origin of the asymmetry was successfully described and a practical way to interpret diffuse diffraction patterns was provided.

Today, the expansion is normally performed out to harmonic terms. Methods of analysis based on the efforts of Borie & Sparks (1971), Tibballs (1975) and Georgopoulos & Cohen (1977) are used to separate the total diffuse intensity into component short-range-order, average-pair-displacement and mean-squared-displacement intensities. The component intensities can be transformed to obtain real-space parameters that describe the local atomic arrangements. These methods have been used for the investigation of short-range order in metallic alloys (Cenedese, Bley & Lefebvre, 1984), vacancy defect clusters in oxides (Hayakawa & Cohen, 1975), Guinier–Preston zones in both binary and ternary aluminium-based alloys (Matsubara & Cohen, 1985; Haeffner & Cohen, 1992), static atomic displacements surrounding interstitial carbon in iron (Butler & Cohen, 1992) and several other systems.

The accuracy of using methods that truncate the Taylor expansion at second order can, in principle, be tested by performing the analysis using both second- and third-order expansions and comparing the results to confirm that the series has converged. Unfortunately, this is difficult, in practice, because the third-order expansion contains more than double the number of component intensities in a second-order expansion. This necessitates a data-set size that may be difficult to collect and that would strain current analysis procedures. Limited versions of this test have been performed by Bubeck & Gerold (1986)

ISSN 0108-7673 ©1993

and Müller, Schönfeld, Kostorz & Bührer (1989), who concluded that the neglect of higher-order terms would introduce unacceptable errors into the determination of the chemical short-range-order parameters. Both of these studies, however, used reciprocal line scans in which the diffuse intensity out to very large scattering vectors had to be included and so were not fair criticisms of the methods currently practised, in which a more restricted reciprocal-space volume is used (Cohen, 1986).

The reliability of using the second-order expansion to determine local-order parameters is tested, in practice, by measuring the diffuse-scattering data in absolute intensity units and comparing the first chemical order parameter with the value unity, as required by definition but not by any numerical constraint. A value close to this would be unlikely to occur by accident, so this parameter can be used as a measure of the accuracy of the local-order diffuse-intensity component. Unfortunately, there is no equivalent test of the reliability of the atomic-displacement diffuse intensity so, at present, one must be satisfied when the diffraction equation, expanded to second order, closely fits the data. A good fit to the data does not, however, guarantee that the displacement parameters that have been solved for are accurate – only that their form can describe the data. It would be reassuring to have some independent means to evaluate this aspect of the method.

In the present study, a computer model of static atomic displacements is used to test the accuracy of the second-order expansion for the particular example of metal-atom distortions in yttria-stabilized cubic zirconium oxide. The model, which contains a realistic distribution of displacements, is used to compute the diffuse intensity exactly. A comparison is then made with calculations based on expansion of the kinematic scattering equation to second, third and higher orders. The use of this computer model allows the entire distribution of displacements (and thus its Fourier transform) to be probed so that a greater insight into the various approximations can be gained. The results of this study can be used as a guide in other systems that contain atomic displacements of similar form.

2. Static-displacement-caused diffuse intensity

The diffuse part of the diffracted intensity from a real crystal can be written simply as the difference between the total intensity, $\mathbf{I}_{\rm tot}(\mathbf{k})$, and the intensity from a hypothetical average crystal, $\mathbf{I}_{\rm ave}(\mathbf{k})$, in which all of the chemical and displacement correlations are replaced with the long-range averages

$$\mathbf{I}_D(\mathbf{k}) = \mathbf{I}_{\rm tot}(\mathbf{k}) - \mathbf{I}_{\rm ave}(\mathbf{k}). \qquad (1)$$

For a multicomponent system, this can be expressed as

$$\mathbf{I}_D(\mathbf{k}) = \sum_{ij}\sum_{lmn} c_i P^{ij}_{lmn} f_i f_j^* \langle \exp[i\mathbf{k}\cdot(\boldsymbol{\delta}^j_{lmn} - \boldsymbol{\delta}^i_o)]\rangle \times \exp(i\mathbf{k}\cdot\mathbf{r}_{lmn}) - \sum_{ij}\sum_{lmn} c_i c_j f_i f_j^* \times \langle \exp[i\mathbf{k}\cdot(\boldsymbol{\delta}^j_\infty - \boldsymbol{\delta}^i_o)]\rangle \exp(i\mathbf{k}\cdot\mathbf{r}_{lmn}). \qquad (2)$$

The summations are over all i and j, which label particular chemical species/sublattice combinations and over all triplets, lmn, which describe allowed interatomic vectors of the average crystal structure. $\mathbf{I}_D(\mathbf{k})$ is the diffuse intensity in electron units per primitive unit cell at scattering wave vector $\mathbf{k}$; P^{ij}_{lmn} is a conditional pair probability describing the likelihood of finding an atom with label j at the end of an interatomic vector $\mathbf{r}_{lmn}$ given an atom with label i at its origin; $\boldsymbol{\delta}^i$ is the displacement of an i atom from its ideal site; the subscripts o and lmn refer to atoms at the origin and end, respectively, of a given interatomic vector and the subscript ∞ refers to a site at long range where displacement correlations are absent; c_i is the sublattice concentration of i, f_i is the atomic scattering factor of the ith component; f_j^* is the complex conjugate of f_j; and lattice averages are indicated by $\langle\ \rangle$.

Equation (2) can be derived directly from the standard kinematic scattering expression simply by replacing the actual identities by their averages (*i.e.* $c_i P^{ij}_{lmn}$) and replacing the exponentials over atomic displacements by average complex exponentials. The pair probabilities and the averages indicated by $\langle\ \rangle$ are to be taken over only the particular sublattice/species combinations indicated by the subscripts and superscripts. The expression $\langle\exp[i\mathbf{k}\cdot(\boldsymbol{\delta}^B_{210} - \boldsymbol{\delta}^A_o)]\rangle$, for example, is the average exponential of the difference between the displacements of atoms of types A and B that are separated by an interatomic vector $\mathbf{r}_{210}$.

It is clear that (2) describes only the diffuse component of the total intensity, because, for distant interatomic vectors, the two summations will cancel. Only those terms involving short-range chemical and/or displacement correlations will contribute and thus $\mathbf{I}_D(\mathbf{k})$ describes features that are broad and extended in reciprocal space exclusively. Likewise, the second term in (2), which describes the scattering from the average crystal structure, contains only sharp Bragg-like features.

Equation (2) can be simplified somewhat by combining the two summations. Explicitly performing the dot products and rewriting in terms of the continuous reciprocal-space coordinates, h_1, h_2 and h_3, one obtains

$$\mathbf{I}_D = \sum_{ij}\sum_{lmn} c_i c_j f_i f_j^* \{(1 - \alpha^{ij}_{lmn}) \times \langle \exp[i2\pi(h_1 X^{ij}_{lmn} + h_2 Y^{ij}_{lmn} + h_3 Z^{ij}_{lmn})]\rangle - \langle \exp[i2\pi(h_1 X^{ij}_{\infty} + h_2 Y^{ij}_{\infty} + h_3 Z^{ij}_{\infty})]\rangle\} \times \exp[i2\pi(h_1 l + h_2 m + h_3 n)]. \qquad (3)$$

Here, the α^{ij}_{lmn} are the Warren short-range-order parameters given by

$$\alpha^{ij}_{lmn} = 1 - (P^{ij}_{lmn}/c_j) \tag{4}$$

and

$$X^{ij}_{lmn} = \delta^{xj}_{lmn} - \delta^{xi}_{o} \quad etc. \tag{5}$$

As discussed in the *Introduction*, to understand and interpret the diffuse intensity from real crystals it often helps to express (3) as a sum of component intensities. This can be done simply by performing a Taylor expansion on the complex exponentials, *i.e.*

$$\langle \exp(a) \rangle = 1 + \langle a \rangle + (1/2!)\langle a^2 \rangle + (1/3!)\langle a^3 \rangle + \ldots, \tag{6}$$

where

$$a = i2\pi(h_1 X^{ij} + h_2 Y^{ij} + h_3 Z^{ij}). \tag{7}$$

Given that

$$\langle [i2\pi(h_1 X^{ij}_{\infty} + h_2 Y^{ij}_{\infty} + h_3 Z^{ij}_{\infty})]^n \rangle = 0 \tag{8}$$

and n is odd, the diffuse intensity, $\mathbf{I}_D$, can be written as

$$\mathbf{I}_D \simeq \mathbf{I}_0 + \mathbf{I}_1 + \mathbf{I}_2 + \mathbf{I}_3 + \ldots, \tag{9}$$

where

$$\mathbf{I}_0 = -\sum_{ij}\sum_{lmn} c_i c_j f_i f_j^* \alpha^{ij}_{lmn} \times \exp[i2\pi(h_1 l + h_2 m + h_3 n)] \tag{10a}$$

$$\mathbf{I}_1 = i2\pi \sum_{ij}\sum_{lmn} c_i c_j f_i f_j^* (1 - \alpha^{ij}_{lmn}) \times \langle (h_1 X^{ij}_{lmn} + h_2 Y^{ij}_{lmn} + h_3 Z^{ij}_{lmn}) \rangle \times \exp[i2\pi(h_1 l + h_2 m + h_3 n)] \tag{10b}$$

$$\mathbf{I}_2 = -2\pi^2 \sum_{ij}\sum_{lmn} c_i c_j f_i f_j^* [(1 - \alpha^{ij}_{lmn}) \times \langle (h_1 X^{ij}_{lmn} + h_2 Y^{ij}_{lmn} + h_3 Z^{ij}_{lmn})^2 \rangle - \langle (h_1 X^{ij}_{\infty} + h_2 Y^{ij}_{\infty} + h_3 Z^{ij}_{\infty})^2 \rangle] \times \exp[i2\pi(h_1 l + h_2 m + h_3 n)] \tag{10c}$$

$$\mathbf{I}_3 = -i(4/3)\pi^3 \sum_{ij}\sum_{lmn} c_i c_j f_i f_j^* (1 - \alpha^{ij}_{lmn}) \times \langle (h_1 X^{ij}_{lmn} + h_2 Y^{ij}_{lmn} + h_3 Z^{ij}_{lmn})^3 \rangle \times \exp[i2\pi(h_1 l + h_2 m + h_3 n)] \tag{10d}$$

etc. Finally, from the indicated products and the fact that each component intensity must be real, (10) can be written

$$\mathbf{I}_0 = -\sum_{ij}\sum_{lmn} c_i c_j f_i f_j^* \alpha^{ij}_{lmn} \times \cos[2\pi(h_1 l + h_2 m + h_3 n)], \tag{11a}$$

$$\mathbf{I}_1 = -2\pi \sum_{ij}\sum_{lmn} c_i c_j f_i f_j^* (1 - \alpha^{ij}_{lmn}) \times [h_1 \langle X^{ij}_{lmn} \rangle + h_2 \langle Y^{ij}_{lmn} \rangle + h_3 \langle Z^{ij}_{lmn} \rangle] \times \sin[2\pi(h_1 l + h_2 m + h_3 n)], \tag{11b}$$

$$\mathbf{I}_2 = -2\pi^2 \sum_{ij}\sum_{lmn} c_i c_j f_i f_j^* (1 - \alpha^{ij}_{lmn}) \times \{h_1^2[\langle (X^{ij}_{lmn})^2 \rangle - (1 - \alpha^{ij}_{lmn})^{-1} \langle (X^{ij}_{\infty})^2 \rangle] + h_2^2[\langle (Y^{ij}_{lmn})^2 \rangle - (1 - \alpha^{ij}_{lmn})^{-1} \langle (Y^{ij}_{\infty})^2 \rangle] + h_3^2[\langle (Z^{ij}_{lmn})^2 \rangle - (1 - \alpha^{ij}_{lmn})^{-1} \langle (Z^{ij}_{\infty})^2 \rangle] + 2h_1 h_2 \langle (X^{ij}_{lmn} Y^{ij}_{lmn}) \rangle + 2h_1 h_3 \langle (X^{ij}_{lmn} Z^{ij}_{lmn}) \rangle + 2h_2 h_3 \langle (Y^{ij}_{lmn} Z^{ij}_{lmn}) \rangle\} \times \cos[2\pi(h_1 l + h_2 m + h_3 n)], \tag{11c}$$

$$\mathbf{I}_3 = (4/3)\pi^3 \sum_{ij}\sum_{lmn} c_i c_j f_i f_j^* (1 - \alpha^{ij}_{lmn}) \times [h_1^3 \langle (X^{ij}_{lmn})^3 \rangle + h_2^3 \langle (Y^{ij}_{lmn})^3 \rangle + h_3^3 \langle (Z^{ij}_{lmn})^3 \rangle + 3h_1^2 h_2 \langle (X^{ij}_{lmn})^2 Y^{ij}_{lmn} \rangle + 3h_1^2 h_3 \langle (X^{ij}_{lmn})^2 Z^{ij}_{lmn} \rangle + 3h_2^2 h_1 \langle (Y^{ij}_{lmn})^2 X^{ij}_{lmn} \rangle + 3h_2^2 h_3 \langle (Y^{ij}_{lmn})^2 Z^{ij}_{lmn} \rangle + 3h_3^2 h_1 \langle (Z^{ij}_{lmn})^2 X^{ij}_{lmn} \rangle + 3h_3^2 h_2 \langle (Z^{ij}_{lmn})^2 Y^{ij}_{lmn} \rangle + 6h_1 h_2 h_3 \langle X^{ij}_{lmn} Y^{ij}_{lmn} Z^{ij}_{lmn} \rangle] \times \sin[2\pi(h_1 l + h_2 m + h_3 n)]. \tag{11d}$$

Some important aspects of (11) should be pointed out here. $\mathbf{I}_0$ describes both the Laue monotonic intensity (corresponding to $lmn = o$) and the well known short-range-order (SRO) diffuse intensity. It is a cosine Fourier sum and thus represents an intensity component that is symmetric about the fundamental reflections. $\mathbf{I}_1$ describes the first-order static-displacement intensity, or the so-called *Warren size-effect intensity*. This term involves a sine Fourier sum and so is antisymmetric, producing the familiar transfer of intensity from one side of a Bragg peak to the other. $\mathbf{I}_2$ represents an intensity component due to mean-squared static atomic displacements. Because this is the first symmetric term that involves static displacements, it contributes to what is commonly called the Huang diffuse intensity. The remaining intensity components are alternately antisymmetric and symmetric about the fundamental reflections and only in the limit of an infinite number of such terms is this expression exact.

Equation (11) is not limited to the description of static-displacement-caused diffuse scattering but can also describe thermal diffuse scattering (TDS) if the indicated averages are taken as temporal as well as spatial. The so called 'first-order TDS' will then appear in the term $\mathbf{I}_2$, the second-order TDS in $\mathbf{I}_4$ *etc.* The present study did not model thermal displacements and so the computed scattering originates from the static displacements only.

Intensity components of higher order than $\mathbf{I}_2$ have not been rigorously included in any studies involving the analysis of full reciprocal-space volumes because an impractical number of component intensities are required even for simple systems. For example, in two-component materials there will be one short-

range-order term, six Warren size-effect terms,* 18 second-order displacement terms and 30 terms associated with the intensity $\mathbf{I}_3$. The inclusion of the 55 terms necessary to describe a binary system using a third-order expansion would strain current experimental and numerical methods.

3. The computer model

In order to probe aspects of the approximation represented by the expansion of (3), a computer model of the metal-atom distortions in yttria-stabilized cubic zirconium oxide, taken from a separate study (Welberry, Butler, Thomson & Withers, 1993), is employed. The model was developed using an interative process in which atomic distortions were applied to the metal lattice (using Monte Carlo techniques) based on a particular arrangement of vacant oxygen sites. The computed diffraction effects from these displacements were then compared with measured diffraction data and the model was improved until a good fit was obtained.

This particular model is a convenient choice for this study because two approximations can be applied to (11) that help to simplify the final interpretation. First, the metal atoms, because of their large scattering power relative to the oxygen lattice, will dominate the scattering, so the diffuse intensity due to oxygen may be left out of the current analysis; second, the scattering-power difference between zirconium and yttrium is at most one electron, so the metal lattice can be treated as if it contains a single atomic species. In this case, the intensities $\mathbf{I}_0$ and $\mathbf{I}_1$ of (11) vanish, the number of terms in $\mathbf{I}_2$ is reduced to six and the number in $\mathbf{I}_3$ to ten. The diffuse intensity can now be written

$$\mathbf{I}_D \simeq \mathbf{I}_2 + \mathbf{I}_3 + \ldots, \tag{12}$$

where

$$\begin{aligned}\mathbf{I}_2 = -2\pi^2 f^2 \sum_{lmn} \{&h_1^2[\langle X_{lmn}^2\rangle - \langle X_\infty^2\rangle] \\ &+ h_2^2(\langle Y_{lmn}^2\rangle - \langle Y_\infty^2\rangle) + h_3^2(\langle Z_{lmn}^2\rangle - \langle Z_\infty^2\rangle) \\ &+ 2h_1h_2\langle X_{lmn}Y_{lmn}\rangle + 2h_1h_3\langle X_{lmn}Z_{lmn}\rangle \\ &+ 2h_2h_3\langle Y_{lmn}Z_{lmn}\rangle\{\cos[2\pi(h_1l + h_2m + h_3n)]\}\end{aligned} \tag{13a}$$

and

$$\begin{aligned}\mathbf{I}_3 = (4/3)\pi^3 f^2 \sum_{lmn} &(h_1^3\langle X_{lmn}^3\rangle + h_2^3\langle Y_{lmn}^3\rangle + h_3^3\langle Z_{lmn}^3\rangle \\ &+ 3h_1^2h_2\langle X_{lmn}^2Y_{lmn}\rangle + 3h_1^2h_3\langle X_{lmn}^2Z_{lmn}\rangle \\ &+ 3h_2^2h_1\langle Y_{lmn}^2X_{lmn}\rangle + 3h_2^2h_3\langle Y_{lmn}^2Z_{lmn}\rangle \\ &+ 3h_3^2h_1\langle Z_{lmn}^2X_{lmn}\rangle + 3h_3^2h_2\langle Z_{lmn}^2Y_{lmn}\rangle \\ &+ 6h_1h_2h_3\langle X_{lmn}Y_{lmn}Z_{lmn}\rangle) \\ &\times \sin[2\pi(h_1l + h_2m + h_3n)].\end{aligned} \tag{13b}$$

Fig. 1(*a*) shows the diffraction pattern of the reciprocal layer $h_3 = 1/2$. It was computed directly from a $32 \times 32 \times 32$ unit-cell computer model of cubic zirconium oxide and is similar to a measurement of the diffuse intensity in this system (Welberry, Withers, Thomson & Butler, 1992). Pair correlations in this simulation did not extend beyond a few unit cells so the computed diffraction images were not affected by the limited size of this simulation. The computation was made using a direct Fourier summation technique (Butler & Welberry, 1992) that is exact within the limits of the model and so corresponds to the case where an infinite number of terms is included in the Taylor expansion. Identical scattering curves were used for both the Zr and Y atoms and only the scattering component due to metal-atom displacements is included so that direct comparison can be made with intensities calculated using (13). Because thermal displacements were not modelled, the scattering curves were not corrected by a thermal Debye–Waller factor. This diffraction image, which is displayed as a grey-scale reproduction of the computed intensity values for clarity, forms the reference to which other calculations, employing the expansion technique, will be compared.

This diffraction pattern has many interesting features. For instance, there are clearly visible 'dark lines', perpendicular to ⟨110⟩, that result from displacement correlations associated with the atomic-size effect (Butler, Withers & Welberry, 1992). Diffuse peaks that lie in pairs either side of the dark lines can also be seen. These maxima in the diffuse intensity result from atomic distortions caused by a locally ordered distribution of oxygen vacancies (Welberry *et al.*, 1993). As in the measured diffraction images, the diffuse peaks nearest to the origin of the reciprocal lattice are significantly weaker than their partners on the opposite side of the dark lines. It was discovered, when the computer model describing these displacements was developed, that the amount of this asymmetry was sensitive to the magnitude of the applied distortions. From this, it was possible to develop a model of the structure in which the displacements should be correct in both magnitude (a 3% r.m.s. distortion was found to be best) and form.

4. Comparison of intensities using second- and third-order expansions

From the computer model, it is simple to calculate the pair displacement averages, $\langle X_{lmn}^2\rangle$, $\langle X_{lmn}^2Y_{lmn}\rangle$

* Note that the nine size-effect terms implicit in (11*b*) for a binary system can be reduced to six by adding the constraint that the average lattice must be satisfied. That is, the weighted average displacements of the *AA*, *AB* and *BB* pairs must sum to zero.

etc., directly for each lattice vector, *lmn*, and so perform the sums indicated in (13). This was done using the same scattering-factor curves as were used in Fig. 1(*a*) and so should reproduce it in both form and absolute magnitude within the limits of the approximation made by truncation of the Taylor expansion. The diffuse intensity computed using only the intensity $\mathbf{I}_2$ of (13) is presented in Fig. 1(*b*). Most features of Fig. 1(*a*) are reproduced in this figure, including the 'dark lines' and the pairs of diffuse peaks on either side of the dark lines. Fig. 1(*b*) does not, however, show an asymmetry in the intensity of the diffuse peaks across the dark lines as is observed in the measured data and the model computation of Fig. 1(*a*). The reason for this is that the intensity term $\mathbf{I}_2$ is a cosine Fourier summation and so can *only* describe a diffuse intensity that is symmetric about planes connecting integer reciprocal positions.

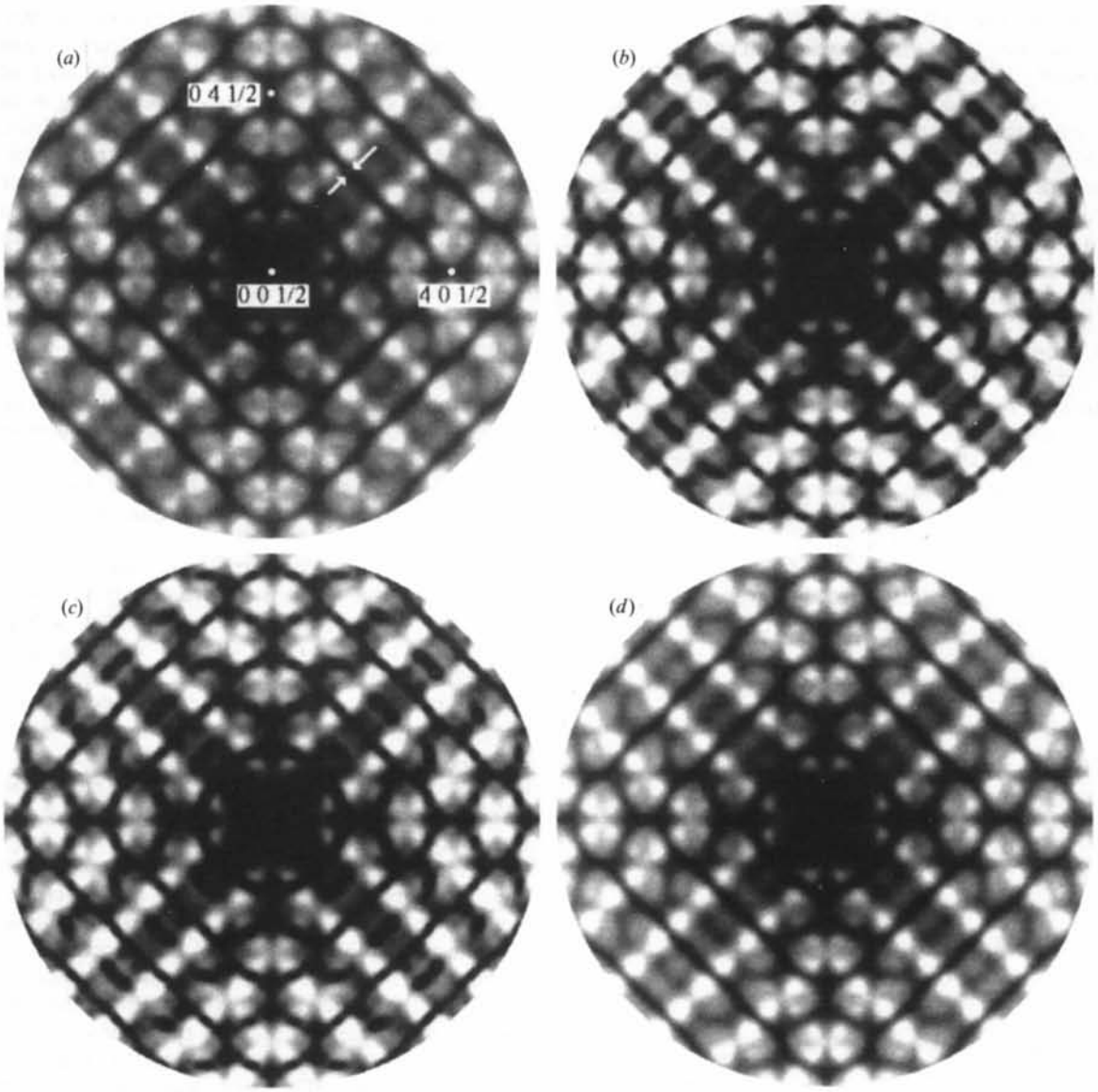

Fig. 1. (*a*) The $h_3 = 1/2$ diffuse section of a computer model of the metal-atom distortions in cubic yttria-stabilized zirconium oxide. This pattern was computed using a direct summation technique that is exact within the limits of the computer model and resembles a measurement of the diffuse intensity. Note the asymmetry in intensity of the diffuse maxima across the dark line indicated by the arrows. (*b*) The same reciprocal section as in (*a*) but computed using only those terms contained in a second-order Taylor expansion. (*c*) The same section computed using terms to third order. (*d*) The same section, computed as in (*a*), but with all atomic distortions reduced by a factor of five. The diffuse asymmetry has now disappeared. (*a*)–(*c*) are displayed on an equivalent linear grey scale such that white corresponds to 375 electron units per metal atom. (*d*) is scaled by an additional factor of 25 so that it can be compared directly with (*b*).

It is thus not possible to reproduce the asymmetry of Fig. 1(*a*) using the diffuse intensity component $\mathbf{I}_2$ alone.

In Fig. 1(*c*), the terms contained in the (antisymmetric) intensity component $\mathbf{I}_3$ have been added to the computation. This diffraction pattern is an improvement over the second-order expansion of Fig. 1(*b*) as the asymmetry in the intensities of the pairs of diffraction maxima separated by the dark lines is now clearly visible. Essentially, all of the diffuse features present in the model diffraction pattern are represented in this figure.

To demonstrate that the observed asymmetry results directly from the magnitude of the atomic distortions present in the model, Fig. 1(*d*) was computed in a manner analogous to Fig. 1(*a*) except that all atomic displacements were reduced by a factor of five. The r.m.s. atomic displacements for this figure are, therefore, only one-fifth the size of those in the original model (0.6% compared with 3%). This diffraction image shows none of the asymmetry apparent in the original model and comparison of Fig. 1(*d*) with Fig. 1(*b*) shows that the approximation made by a second-order expansion, when the displacements are less than 1%, is accurate across the whole reciprocal section shown.

5. Quantitative comparison

From the original (3% distortion) computer model, it is evident that, while all of the major qualitative features of the diffraction pattern have been reproduced by using an expansion to third order, there remains a large quantitative discrepancy between Figs. 1(*a*) and (*c*). This is shown clearly by the saturation of the diffuse maxima, which is most pronounced at the highest diffraction angles. (Note that the calculation scales, data plotting and photographic reproductions of these figures were identical.) When comparison is made close to the reciprocal origin, there is little apparent difference, but beyond the dark band connecting the 4,0,1/2 and 0,4,1/2 positions the effect becomes quite noticeable. At this stage, the accuracy of using an expansion to only third order begins to degrade significantly.

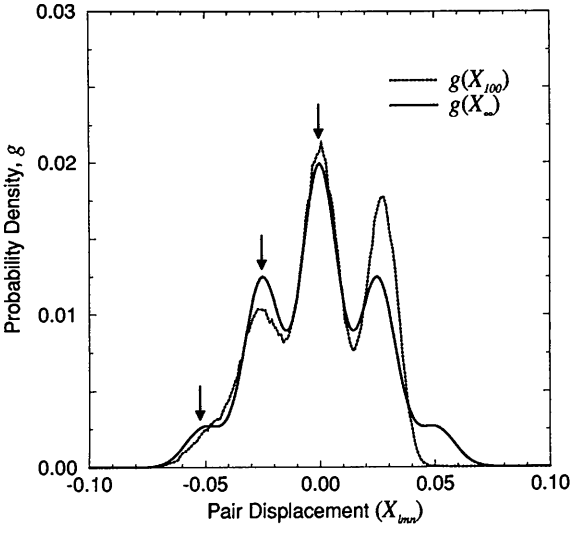

Fig. 2. The pair displacement distribution functions for long-range (uncorrelated) atom pairs and for near-neighbour atom pairs separated by ⟨100⟩ taken from the computer model. The arrows indicate the three maxima in the long-range trimodal distribution explained in the text.

To understand where this approximation breaks down, it helps to isolate one term of the expansion and study how each expansion order contributes to it. This can be done conveniently for the interatomic vector $lmn = 100$, which makes a large contribution to the total diffuse intensity. To simplify the present discussion, consider the contribution of this interatomic vector along the reciprocal line where $h_2 = h_3 = 0$. Here, the Taylor-expansion approximation can be written

$$\langle \exp(i2\pi h_1 X_{100})\rangle - \langle \exp(i2\pi h_1 X_\infty)\rangle = -2\pi^2 h_1^2(\langle X_{100}^2\rangle - \langle X_\infty^2\rangle) + i(4/3)\pi^3 h_1^3\langle X_{100}^3\rangle + \ldots . \quad (14)$$

The terms on the left-hand side of (14) are Fourier transforms (of the x components) of the displacement distribution functions of atom pairs separated by near-neighbour 100 and long-range lattice vectors, respectively. These two distributions, which we label $g(X_{100})$ and $g(X_\infty)$, are shown in Fig. 2.

Contrary to what might initially be expected, the long-range (uncorrelated) pair-displacement distribution given by the solid line in this figure is not a simple single-peaked function but contains three main maxima, indicated by arrows. This trimodal distribution occurs because the metal atoms in the computer model have, mainly, two distinct local environments. A particular metal atom will either be coordinated by a completely filled shell of near-neighbour oxygen atoms or it will lie near to one or more vacant oxygen sites. In the latter case, the metal-atom displacement will be controlled by direct near-neighbour interactions and so will be large as otherwise the displacements will result from more indirect effects and will be small. The three peaks in the pair-distribution function correspond to neither atom, one atom or both atoms of the pair having oxygen-vacancy near neighbours. The form of this pair-displacement distribution function arises simply because a metal atom is either near a lattice 'defect' or is not. Multimodal distribution functions like this one will therefore be likely to occur in many crystals that contain defects.

The distribution $g(X_\infty)$ is symmetric because the long-range average cubic symmetry of the crystal must be retained. The Fourier transform of this

distribution will contain only real (symmetric) components. The distribution $g(X_{100})$ is more general and so will contain both real (symmetric) and imaginary (antisymmetric) components. The right-hand side of (14) describes the difference between these two transforms as a polynomial function of the reciprocal coordinate h_1.

The difference Fourier transforms of the distribution functions displayed in Fig. 2 were computed out to $h_1 = 6$ and are presented as solid curves in Figs. 3(*a*) (symmetric component) and (*b*) (antisymmetric component). These curves are compared with those computed using a Taylor-expansion approximation out to various orders. Both figures have been given the same vertical scale. The *quantitative* accuracy of the Taylor expansion is thus clearly displayed in this figure. A second-order expansion accurately describes the symmetric part of the transform out to about $h_1 = 3$ but at $h_1 = 5$ it is in error by nearly 50%. An expansion to the fourth order approximates the real part of the transform very well out to $h_1 = 5$ (now the error is reduced to only 5%) and a sixth-order expansion is nearly indistinguishable from the exact transform over the full range of the figure.

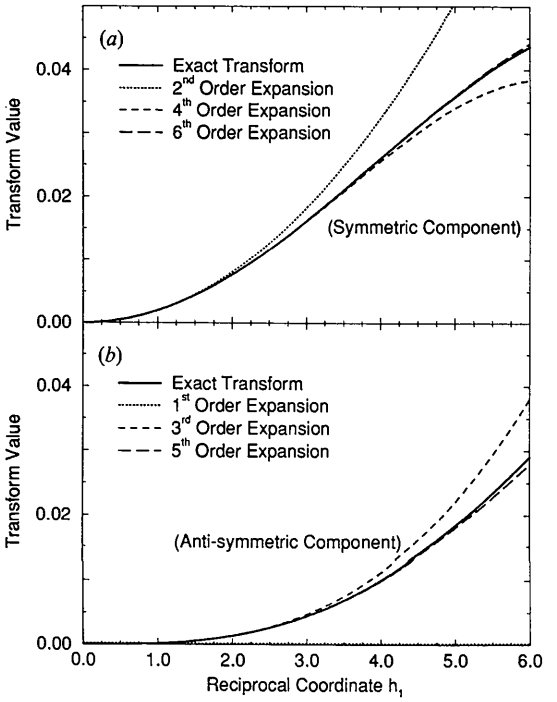

Fig. 3. The symmetric and antisymmetric parts of the Fourier transform of the difference between the two distribution functions of Fig. 2 along the $\langle h_1 00\rangle$ reciprocal-space direction. The solid line represents the exact transform and the broken lines indicate Taylor-expansion approximations to various orders. Even and odd terms in the expansion contribute only to the symmetric and the antisymmetric parts, respectively, of the transform.

As discussed earlier, an expansion to second order does not contain any antisymmetric components because the first-order term cannot contribute in this example. At $h_1 = 3$, this antisymmetric component contributes 28% to the total (of the $lmn = 100$ term). At $h_1 = 4$, this has risen to nearly 40% of the total and can no longer be ignored. Inclusion of a third-order term in the expansion improves the situation a great deal and an accurate description of the antisymmetric part of the transform out to $h_1 = 4$ is obtained. The addition of a fifth-order term to the expansion gives an accurate quantitative fit out to $h_1 = 6$ (near the physical limit of measurement when using Cu $K\alpha$ radiation).

6. Concluding remarks

An average 3% static atomic distortion is larger than would be found in many systems where the Taylor expansion has been employed, such as most short-range-ordered alloys, where typical atomic displacements are nearer to 1%. But, for materials such as stabilized zirconium oxide, which has a large proportion of oxygen vacancies (10%), and crystals that are dominated by defect clusters, the displacements are often of this magnitude. In these cases, the results from this study can be used as a guide in estimating an appropriate experimental upper limit to the diffraction angle where the expansion approximation remains valid.

In the yttria-stabilized zirconium oxide example, the metal-atom diffraction contrast is minimal so most of the diffuse scattering can be attributed to displacement terms of second or higher order. In this instance, any errors resulting from truncation of the Taylor expansion are magnified – and, if the expansion is made only to second order, the scattering equation cannot even describe the diffuse asymmetry that is one of the defining features of the diffraction pattern of Fig. 1(*a*). However, in crystals where there is a large scattering contrast, the diffuse intensities $\mathbf{I}_0$ (short-range-order scattering) and $\mathbf{I}_1$ may dominate the diffraction pattern and lessen the impact caused by neglect of higher-order displacement terms.

The consequences of neglecting these higher-order terms will also vary with the form of the pair displacement distribution functions that exist in the material under study. For instance, if these distributions are broad but symmetric, the intensity $\mathbf{I}_3$ will be negligible but $\mathbf{I}_4$ could be significant. Multimodal distributions, like the one shown in Fig. 2, will probably be found in many systems where two or more distinct local atomic environments exist. The results from this study will most generally apply to such crystals.

Unfortunately, it is not possible to analyse directly diffuse-scattering data using (3) because the reciprocal coordinates are contained inside the average

exponentials and the displacement distribution functions are not known. Also, the geometric growth in the number of terms in the Taylor expansion severely restricts the order to which this expansion can be successfully applied to real diffraction data. Therefore, when the displacements are large, the Taylor expansion must be abandoned in favour of methods based on direct simulation of the defects or perhaps other (nonlinear) descriptions of the diffuse intensity, for instance one based on a cumulant expansion of the exponential.

The displacement correlation parameters that arise naturally in the Taylor-expansion description should not be forgotten entirely even in such instances, because these parameters are convenient to use in the *qualitative* description of displacement disorder and can thus aid understanding of the origins of many diffuse features. For example, the Warren size-effect intensity contains parameters that describe the deviations of pair distances from the long-range average and give rise to an easily interpreted diffuse asymmetry. The forms of the displacement correlation parameters associated with the intensity $\mathbf{I}_2$ have also recently been used to describe successfully the diffuse absences that are evident in some diffraction patterns, such as those present in the diffraction image of Fig. 1(*a*) (Butler, Withers & Welberry, 1992).

The authors thank Dr R. L. Withers for valuable discussions during the preparation of this manuscript. The diffuse-scattering images of Figs. 1(*a*) and (*d*) were computed on a Fujitsu VP-2200 supercomputer using a grant from the Australian National University Supercomputer Facility.

References

BORIE, B. & SPARKS, C. J. (1971). *Acta Cryst.* A**27**, 198–201.
BUBECK, E. & GEROLD, V. (1986). *J. Appl. Cryst.* **19**, 164–167.
BUTLER, B. D. & COHEN, J. B. (1992). *Acta Metall. Mater.* **41**, 41–48.
BUTLER, B. D. & WELBERRY, T. R. (1992). *J. Appl. Cryst.* **25**, 391–399.
BUTLER, B. D., WITHERS, R. L. & WELBERRY, T. R. (1992). *Acta Cryst.* A**48**, 737–746.
CENEDESE, P., BLEY, F. & LEFEBVRE, S. (1984). *Acta Cryst.* A**40**, 228–240.
COHEN, J. B. (1986). *J. Appl. Cryst.* **19**, 491.
COWLEY, J. M. (1950). *J. Appl. Phys.* **21**, 24.
GEORGOPOULOS, P. & COHEN, J. B. (1977). *J. Phys. (Paris)*, C7, **38**, 191–196.
HAEFFNER, D. R. & COHEN, J. B. (1992). *Acta Metall. Mater.* **40**, 831–838.
HAYAKAWA, M. & COHEN, J. B. (1975). *Acta Cryst.* A**31**, 635–645.
MATSUBARA, E. & COHEN, J. B. (1985). *Acta Metall.* **33**, 1945–1955.
MÜLLER, P. P., SCHÖNFELD, B., KOSTORZ, G. & BÜHRER, W. (1989). *Acta Metall.* **37**, 2125–2132.
TIBBALLS, J. E. (1975). *J. Appl. Cryst.* **8**, 111–114.
WARREN, B. E., AVERBACH, B. L. & ROBERTS, B. W. (1951). *J. Appl. Phys.* **22**, 1493–1496.
WELBERRY, T. R., BUTLER, B. D., THOMSON, J. G. & WITHERS, R. L. (1993). *J. Solid State Chem.* In the press.
WELBERRY, T. R., WITHERS, R. L., THOMSON, J. G. & BUTLER, B. D. (1992). *J. Solid State Chem.* **100**, 71–89.

Acta Cryst. (1993). A**49**, 743–749

Modulated Anomalous X-ray Scattering*

BY PETE R. JEMIAN, JOHN E. ENDERBY,† ANDREW MERRIAM,‡ DAVID L. PRICE AND MARIE-LOUISE SABOUNGI

Materials Science Division, Argonne National Laboratory, Argonne, IL 60439, *USA*

(*Received* 2 *October* 1992; *accepted* 18 *March* 1993)

Abstract

To determine the partial structure associated with a particular element in a multicomponent system, contrast variation is proposed based on the use of modulated anomalous X-ray scattering (MAXS). The photon energy of the X-ray beam incident on the sample is modulated over a range of energies below an absorption edge of the selected element. Because of anomalous dispersion, measurement of the scattered-intensity gradient with respect to the energy gives the required information. MAXS can be used in both small-angle and wide-angle diffraction and is applicable, in principle, to crystalline, amorphous and liquid materials. Energy modulation obtained by oscillating the Bragg angle of the monochromator by a small amount, followed by phase-sensitive detection, leads to a significant reduction of both systematic and statistical errors. Results of a

* This work was performed under the auspices of the US Department of Energy, Division of Materials Science, Office of Basic Energy Sciences, under contract W-31-109-ENG-38.

† Permanent address: H. H. Wills Physics Laboratory, Tyndall Avenue, University of Bristol, Bristol BS8 1TL, England.

‡ Undergraduate research participant (Department of Educational Programs, ANL). Present address: Department of Applied Physics, Stanford University, CA, USA.